Acta Neuropathologica Communications

RESEARCH

Open Access

Investigating genotype-phenotype correlation of limb-girdle muscular dystrophy R8: association of clinical severity, protein biological function and protein oligomerization

Xiongda Liang[1], Jiameng Si[1], Hongting Xie[1], Yuqing Guan[2,3], Wanying Lin[4], Zezhang Lin[1], Ganwei Zheng[1], Xiaofeng Wei[1], Xingbang Xiong[5], Zhengfei Zhuang[5] and Xuan Shang[1,6*]

Abstract

Limb-girdle muscular dystrophy R8 (LGMD R8) is a hereditary muscle disease caused by biallelic defects in E3 ubiquitinated ligase gene (TRIM32). LGMD R8 is featured by high genetic heterogeneity and phenotypic diversity, most pathogenic variants are missense variants located in the NHL domain, but the genotype-phenotype correlation remains unclear. We hypothesized that various missense variants in NHL domain might have different degrees of impact on the structure and function of the protein, thus resulting in disease variability. Firstly, by analyzing present patients' clinical data, we screen out 4 variants: R394H, D487N, V591M and P619S. Patients homozygous for the aforementioned variants exhibited significant phenotypic variability, including variations in age of onset and age of any walking aid (AWA). Then, bioinformatics analysis, cellular functional experiment and biophysical assay were used to measure the effect of above variants in TRIM32 protein oligomerization and ubiquitination to target substrates. And they revealed distinct differences in the intrinsic E3 ligase activity among various mutant TRIM32 proteins, which corresponded to differences in their oligomerization status. In conclusion, our results showed a correlation between clinical severity, protein function and oligomerization state in patients homozygous for missense variants in NHL domain. It is the first time to reveal a connection between TRIM32 variant with LGMD R8 phenotype and this finding provided valuable reference in predicting disease severity and more precise guidance to affected family on genetic counseling.

Keywords Genotype-phenotype correlation, LGMD R8, NHL domain, Oligomerization, TRIM32

*Correspondence:
Xuan Shang
shangrabbit@163.com
[1]Department of Medical Genetics, School of Basic Medical Science, Southern Medical University, Guangzhou 510515, China
[2]Department of Neurology, Nanfang Hospital, Southern Medical University, Guangzhou, China
[3]Department of Neurology, Ganzhou People's Hospital, Ganzhou, China
[4]Department of Laboratory Medicine, Nanfang Hospital, Southern Medical University, Guangzhou, China
[5]College of Biophotonics, South China Normal University, Guangzhou, China
[6]Innovation Center for Diagnostics and Treatment of Thalassemia, Nanfang Hospital, Southern Medical University, Guangzhou, China

Introduction

The limb-girdle muscular dystrophies (LGMDs) are a group of genetic disorders characterized by weakness and wasting in the pelvic and shoulder areas. Over 30 subtypes of LGMD have been identified, including 5 dominant and 26 recessive forms [1]. The prevalence of LGMDs is estimated to range from 0.8 to 6 per 100,000, making it the fourth most common genetic neuromuscular disease [2]. LGMD R8, a progressive autosomal recessive muscular dystrophy, was first described in the Manitoba Hutterite population [3]. Patients with LGMD R8 typically present with proximal muscle weakness, atrophic wasting of the lower extremities, and elevated creatine kinase (CK) levels [4]. Cardiac or facial involvement is uncommon. Although fewer than 100 cases have been reported to date, these cases have exhibited highly variable clinical severity, ranging from increased serum CK levels without apparent muscular impairment to severe muscle weakness resulting in wheelchair dependence [5]. Disease onset is generally in the second or third decade of life, with earlier onset associated with more severe clinical phenotypes, the faster rate of progression and being more disabling [1].

LGMD R8 is caused by variants in the TRIM32 gene. The TRIM32 protein functions as an E3 ubiquitin ligase, catalyzing the transfer of ubiquitin (Ub) to target proteins within the Ub-proteasome pathway [6, 7]. TRIM32 shows broad E3 ligase activity as it can ubiquitinate itself and many other substrates to mediate and regulate many physiological and pathophysiological processes in different cell types, such as growth, differentiation, regeneration, immunity and carcinogenesis [8]. Structurally, the TRIM32 protein comprises a RING domain, a B-box domain, a coiled-coil domain, and six NHL domains from the N- to the C-terminal ends [9]. Variants in TRIM32 gene result in two clinically diverse diseases. A variant in the B-box domain (p.P130S) leads to Bardet-Biedl syndrome (BBS), a complex non-myopathic disorder characterized by retinal dystrophy, obesity, kidney abnormalities and polydactyly [10]. In contrast, variants in other regions of the gene are generally associated with LGMD R8. Intriguingly, no muscle abnormality is found in BBS patients, suggesting that variants in different domains of the TRIM32 protein have distinct effects on its function, leading to differential disease phenotypes through varied pathogenic mechanisms.

To date, approximately 80 LGMD R8 patients have been reported. More than 30 point variants and 7 deletions in TRIM32 gene have been identified in these patients, and their clinical manifestation ranged widely from nearly asymptomatic to more severe, wheelchair-bound conditions [11]. This data underscored the parallel between clinical heterogeneity and molecular heterogeneity. Point variants in NHL domains were the most common cause of LGMD R8, and patients carrying two variants in NHL repeats typically presented more severe symptoms than other patients [11]. However, a clear genotype-phenotype correlation has not been fully elucidated, making it challenging for clinicians to predict disease severity in childhood and to provide accurate family counseling.

Homozygotes of missense variants in the NHL domains constitute the largest group of current LGMD R8 cases. Therefore, we intend to explore genotype-phenotype correlation within this group first. In this research, considering that the NHL domain primarily mediates TRIM32 oligomerization and that oligomerization status affects E3 ligase activity [12], we hypothesized that various variants in the NHL domain lead to abnormal protein oligomerization, resulting in impaired interaction and ubiquitination with key substrates in maintenance of muscle homeostasis, thereby causing progressive weakness in skeletal muscle [7]. In such condition, the clinical phenotype of LGMDR8 was directly related to the extent of protein oligomerization in cells. Thus, the quantitative determination of oligomerization ability by relevant assays could be used as an effective indicator of disease severity.

Materials and methods

Patients

An electronic literature search in the PubMed database using "TRIM32", "LGMD", "LGMD 2H" or "LGMD R8" as keywords and all reported cases with detailed genotype and clinical data were collected. Totally 82 patients (67 homozygotes and 15 compound heterozygotes) were enrolled here (Supplementary Table S1).

Protein modeling

To predict the structural and functional consequences of missense TRIM32 mutants, protein structure analysis was performed. The PDB file of 3D model of wild-type (WT) protein was downloaded from AlphaFold protein structure database (https://alphafold.ebi.ac.uk/). Then 3D models of each mutant protein were constructed by Swiss-Model software using the predicted WT protein model from AlphaFold as a template. The generated PDB files were imported into PyMOL for model visualization and structure analysis. To predict stability changes in protein variants, we used the FoldX plugin for the YASARA software. The ΔΔG free-energy change was calculated as the difference between the folded and unfolded free-energy states (ΔGmutant– ΔGwild-type) [13].

Plasmid construction

The coding sequence of TRIM32 was acquired from healthy individual complementary DNA (cDNA) and separately cloned into the green fluorescent pEGFP-N1 vector, red fluorescent pmCherry-N1 vector, PHAGE-3×Flag

vector, enhanced cyan fluorescence pECFP-N1vector and enhanced yellow fluorescence pEYFP-N1 vector: pEGFP-N1-TRIM32-WT, mCherry-N1-TRIM32-WT, PHAGE-TRIM32-3×Flag, pECFP-N1-TRIM32-WT and pEYFP-N1-TRIM32-WT. Next, 5 pairs of complementary primers were used to construct the mutant expression vectors with p.P130S, p.R394H, p.D487N, p.V591M and p.P619S variants by site-directed mutagenesis.

(P130S: 5'-AGTTTGTAGTAACCAATGTGGAAGGT GGAA-3';

R394H: 5'-TCGCCAGATTAGCCGCTTCTTCTCGG AGAA-3';

D487N: 5'-AGTTTGTAGTAACCAATGTGGAAGGT GGAA-3';

V591M: 5'-AGTTTGTAGTAACCAATGTGGAAGGT GGAA-3';

P619S: 5'-AGTTTGTAGTAACCAATGTGGAAGGTG GAA-3').

In addition, the coding sequences of NDRG2 and ULK1 were separately cloned into the PHAGE-3×Flag vector: PHAGE-NDRG2-3×Flag and PHAGE-ULK1-3×Flag. The ubiquitin expression vector pcDNA3-HA-Ubiquitin-WT was purchased from Miaoling Biology (Wuhan, China).

Cell culture and transfection

Human embryonic kidney (HEK)-293T cells were cultured in 10% fetal bovine serum (FBS, Excell, Shanghai, China), 90% DMEM cell medium (Gibco, USA) and 1% penicillin and streptomycin (Gibco, USA) at 37 °C and 5% CO2. When the cells reached 60–70% confluence, 3 μg of WT pEGFP-N1-TRIM32 plasmid, 5 mutant pEGFP-N1-TRIM32 plasmids were transiently transfected into HEK-293T cells by using Lipofectamine 2000 (Thermo Fisher Scientific, USA). In addition, pmCherry-N1-TRIM32-WT plasmid and mutant pEGFP-N1-TRIM32 plasmids were also transiently co-transfected into HEK-293T cells at a concentration ratio of 1:1. Live cell fluorescence was observed at 24 h after transfection.

Co-immunoprecipitation

When the cells reached 70–80% confluence, the PHAGE-TRIM32-3×Flag and of WT and mutant-type were co-transferred with their EGFP-tagged counterparts into HEK-293T cells in 10 cm dishes. In addition, all pEGFP-N1-TRIM32 plasmids were co-transfected with PHAGE-NDRG2-3×Flag/PHAGE-ULK1-3×Flag plasmids and pcDNA3-HA-Ubiquitin-WT plasmids into HEK-293T cells in 10 cm dishes, respectively. After 24 h transfection, HEK-293T cells were lysed in NP40 buffer (Beyotime, Shanghai, China) with protease inhibitor (Beyotime, Shanghai, China) for 30 min, centrifuged at 12,000 rpm for 10 min at 4℃ and the supernatants were collected of total lysates, then a part was taken out as a positive control and the rest was immunoprecipitated with anti-Flag antibody magnetic beads (Mabnus, Wuhan, China) at 4 ℃ for 16 h. Finally, all protein samples were boiled for 5 min 95℃ in 1×SDS standard loading buffer (Fdbio science, Hangzhou, China) before western blotting detection.

Western blotting analysis

The protein samples were separated by 10% SDS-PAGE, electrophoretically transferred onto 0.22 μm polyvinylidene difluoride membranes. After blocking with 5% skimmed milk at room temperature for 2 h, according to the molecular weight of the proteins, the membrane was cut at appropriate positions and incubated overnight at 4 ℃with antibodies: Flag antibody (1:2000, Proteintech, USA, 20543-1-AP), GFP antibody (1:2000, Proteintech, USA, 66002-1-Ig), and HA antibody (1:1000, Proteintech, USA, 51064-2-AP). After washing three times with TBST, the membranes were incubated with HRP-labeled goat anti-rabbit polyclonal antibody (1: 10000, Proteintech, USA, SA00001-2) at room temperature for 2 h. After washing with TBST buffer, the immunoreactive bands were visualized by enhanced chemiluminescence chemistry substrate (Fdbio science, Hangzhou, China).

Quantitative FRET imaging

Cells were co-transfected with 200 ng of plasmid encoding CFP-tagged protein and various concentrations (200, 400, 600, and 800 ng, respectively) of plasmid encoding YFP-tagged protein. Quantitative FRET imaging was performed on a fluorescence microscope (Axio Observer 7, Carl Zeiss). IDD(DA), IAA(DA), and IDA(DA) raw images were acquired by utilizing distinctive excitation/emission filters j Donor-centric FRET efficiency (E_D) and acceptor–donor ratio (Rc) were measured by using FRET method just as described previously [14, 15].

ED saturation assay

Only the cells with fluorescence signals at least three times higher than backgrounds and < 60,000 (the saturation value of fluorescence signal is 65,535) were chosen for analysis. E_D values were distributed into bins of different sizes according to concentration ratio of total acceptor-to-donor (Rc) and plotted against Rc. The saturation binding curves were fitted using Origin with the function: $E_D = E_D\max \times Rc/(Kd + Rc)$. $E_D\max$ is the maximum E_D corresponding to saturation of donor binding sites by an acceptor and Kd is the relative equilibrium dissociation constant [16, 17].

Statistical analysis

Statistical differences between groups were determined by students' T-tests and statistical correlation between groups was determined by linear correlation analysis. The quantified results are shown as the means ± SEMs.

Statistical significance was determined by a *P* value of less than 0.05. All statistical analyses were performed using the statistical software SPSS25 and GraphPad Prism 7.

Results

Difference in ages of onset and AWA showed the gradient phenotypic divergence in LGMD R8 patients

After reviewing all published literature related to TRIM32, a total of 82 LGMD R8patients were enrolled in the study, including 67 homozygotes (81.7%) and 15 compound heterozygotes (18.3%) (Supplementary Table S1). Their detailed clinical data was collected and three important indices (age of onset, AWA, serum CK level) were summarized. It should be noted that data for all three indices were not available for all patients in the publications. Among these 82 patients, 80 patients were reported with age of onset, 24 patients were reported with AWA, and 71 patients were reported with CK level (Fig. 1A). The age of onset ranged from childhood to late adulthood (3 years– 63 years). The CK level ranged from 120U/L to 6500U/L, which is up to 32.5 times the upper limit of the normal value (200 U/L). In the relatively severe patients who loss independent ambulation ability due to proximal muscle weakness, the age required wheelchair or other walking aid (AWA) ranged from 20-years-old to more than 60-years-old. Hence, according to present data, the phenotypic variability was large among the LGMDR8 cohort, from milder forms with late onset and slower progression to severe forms with early onset disease that progresses rapidly and results in early loss of ambulation.

A high genetic heterogeneity was also observed in these 82 patients. There are multiple genotypes, with some genotypes represented by only a single patient (Supplementary Table S1). Due to the limited number of cases, elucidating the genotype-phenotype correlation for the entire LGMD R8 cohort was challenging. Based on the type and location of variants, the 82 patients were divided into 8 groups (Figure S1). Homozygotes of missense variants in NHL domains were the largest group, including 56 reported cases: 2 of R394H, 48 of D487N, 3 of V591M and one case of I395T, R596G and P619S. Interestingly, regarding the key index of disease severity (age of onset and AWA), above cases displayed gradient phenotypic divergence (Fig. 1B). Patients with R394H and I395T variants presented mild phenotype with the latest onset age and AWA. Patients with D487N variant had an intermediate onset age, in youth, and they almost dependent on wheelchairs to travel during middle age. Patients with V591M, R596G and P619S variants showed severe phenotype, with the earliest onset age, in adolescence, which is on average 22 years earlier than that of patients with R394H variant. These patients also experienced rapid disease progression, depending on wheelchairs during thirties, which is on average 28 years earlier than that of patients with R394H variant. Since I395T and R596G were each detected in only one case, and their locations were very close to R394H and V591M, respectively, we ultimately selected four variants (R394H, D487N, V591M, P619S) for further research (Fig. 1C). According to the clinical data displayed in Fig. 1B, the order of disease severity, from mild to severe, was R394H < D487N < V591M/P619S.

Prediction of structural changes and instability in the TRIM32 protein caused by the variants

NHL domain was regarded to play a key role in TRIM32 protein self-oligomerization and enhance substrate binding [12]. Alteration of NHL repeats may induce changes in the 3D structure, thus affects protein biological functions. Consequently, we used in silico studies to predict the molecular consequences of 4 aforementioned missense variants (R394H, D487N, V591M and P619S) and tried to measure their structural damage effect by the computational tools. The AlphaFold system, along with recently resolved experimental structures of TRIM32 NHL repeats, was utilized to showed the physically observable changes in the 3D models caused by the variants. A numerical way, ΔΔG calculation, was used to estimate thermodynamic stability changes due to the amino acid substitution. An increase in the ΔΔG value indicates a rise in structural instability.

As shown in Figs. 1D, 4 missense variants all resulted in substantial structural damage. The R394H variant led to a missing H-bond with E406 due to the substitution (Fig. 1E). The D487N variant induced the formation of new H-bond with Q468 but also resulted in the breakage of more H-bonds in E489 and S470 (Fig. 1F). The V591M variant and P619S variant caused a loss of α-helix or β-sheet elements respectively and both variants introduced a buried hydrophilic residue with an expected destabilizing effect (Fig. 1G-H). The stability analysis suggested that all the missense variants were particularly destabilizing, with ΔΔG > 5. Notably, according to the result in Fig. 1D, the predicted structural changes and instability impacts of the 4 variants were proportional to disease severity observed in the corresponding homozygous patients, which indicating a potential correlation between phenotypic severity and changes in protein structure and stability induced by these variations.

The function of ubiquitinating target substrates was impaired in mutant TRIM32 proteins

The modeling analysis suggested that above 4 variants resulted in variable damage impact on protein structure and stability. Since NHL repeats are essential for mediating protein–protein interactions and ensuring the binding and ubiquitination of specific substrates, we

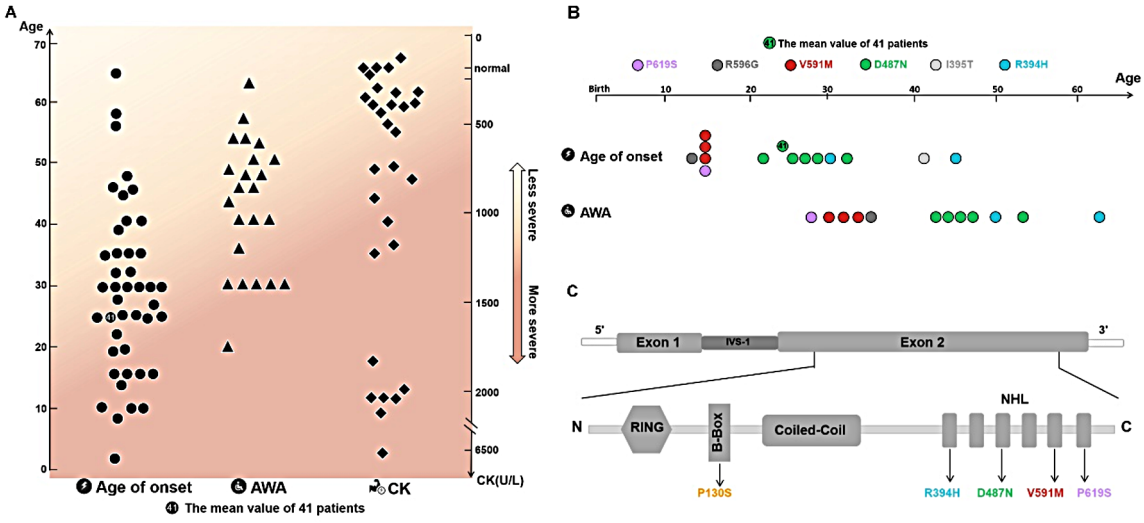

D

Domain	Variant	ΔΔG(kcal/mol)	Protein structural changes
1st NHL	R394H	+5.01	Broken H bond
3rd NHL	D487N	+11.65	Broken H bond, new H bond introduced
5th NHL	V591M	+22.19	Lost α-helix, hydrophilic introduced
6th NHL	P619S	+23.41	Lost β-sheet, hydrophilic introduced

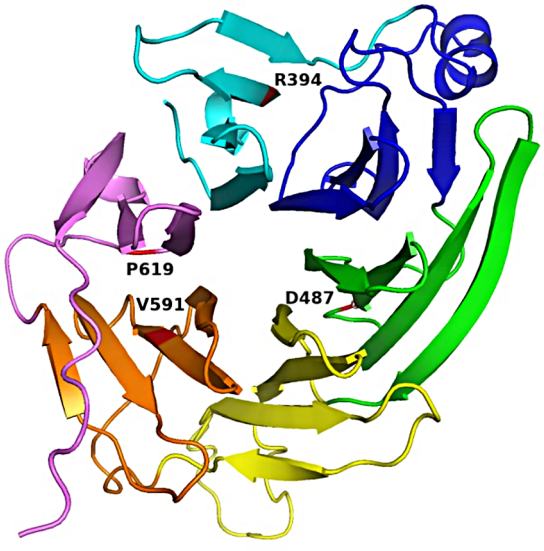

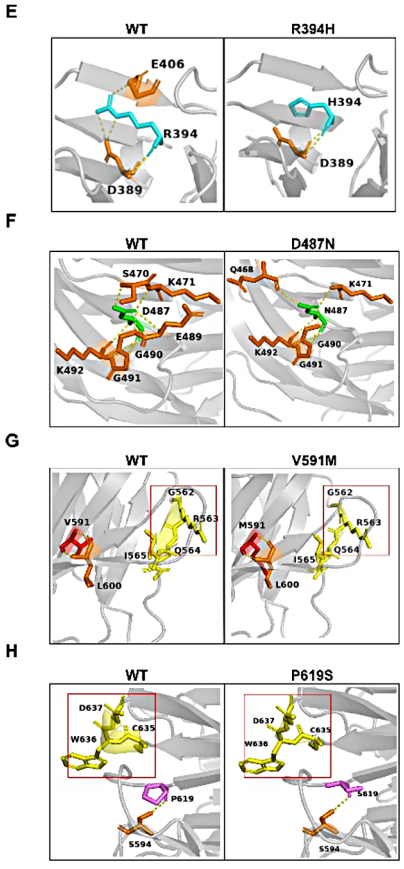

Fig. 1 Clinical phenotype analysis of LGMDR8 patients and prediction of structural changes and instability in the TRIM32 protein caused by the 4 missense variants. (**A**) Summary of the onset age, AWA and CK level in known patients. (**B**) Patients with homozygous missense variants in the NHL domain are arranged according to two timelines: Age of onset and Age of any walking aid (AWA). Dot with 41 in (**A**) and (**B**) represents the mean value of 41 patients who are homozygotes of D487N. (**C**) The schematic of 4 selected missense variants location on TRIM32 protein. (**D**) Structure analysis and ΔΔG calculation of TRIM32 missense variants. ΔΔG is the measure of the free energy change due to an amino acid substitution. ΔΔG ≥ 1, the substitution is defined as destabilizing (**E**) R394H results in H-bond with E406 breakage. (**F**) D487N leads to a new H-bond introduction and H-bonds breakage in E489 and S470. (**G**) V591M causes a loss of α-helix and replaces hydrophobic valine with a hydrophilic methionine. (**H**) P619S causes a loss of β-sheet and replaces hydrophobic proline with a hydrophilic serine. Red box indicates their conformational difference

performed co-immunoprecipitation (Co-IP) and Western blot experiments to assess whether the biochemical function of mutant TRIM32 protein was impaired. Two key substrates involved in muscle homeostasis were selected for testing: ULK1, which is related to muscle atrophy [18], and NDRG2, which is related to muscle regeneration [19]. The WT and the P130S variant in the B-box region, which is causative for BBS, were used as controls. GFP-tagged TRIM32 (WT or mutants), FLAG-tagged substrates (ULK1 or NDRG2) and HA-tagged ubiquitin were co-expressed in HEK-293 cells. Anti-GFP and anti-FLAG antibodies were used for Co-IP assay, anti-HA antibody was used for ubiquitination assay.

We found that only TRIM32-WT and TRIM32-P130S mutants co-immunoprecipitated with NDRG2, indicating the interaction occurred, while the binding of other 4 missense mutants (R394H, D487N, V591M and P619S) with NDRG2 was severely affected. In addition, the ubiquitination ability of these mutants was also significantly impaired, as evidenced by the very weak ubiquitin signal detected in their channels (Fig. 2A). However, in the Co-IP experiment of ULK1, we found that different TRIM32 mutants differentially affected the interaction and ubiquitination of ULK1. The interaction effect and ubiquitination activity of P130S were equal to WT, while the other 4 mutants showed significantly attenuated effects. R394H mutant was the least affected and could interact with ULK1 and ubiquitinate it. D487N mutant was weakly interacted with ULK1, with reduced ubiquitination ability. V591M and P619S proteins had the most severe impact, being almost unable to interact with ULK1, their ubiquitination ability was nearly defective (Fig. 2B). Based on this result, a corresponding relationship was also noticed between phenotypic severity and the extents of biochemical function changes caused by the 4 missense variants.

Mutant TRIM32 proteins affected the formation of cytoplasmic bodies

One feature of TRIM32 protein is that it can interact with itself to form oligomers, and the oligomeric state is linked to catalytic activity. The ability of oligomerization is also called as self-association. At the subcellular level, previous researches [20–22] had revealed three things: (1) Substrate binding induces the formation of higher-order oligomers of TRIM32, further enhancing its E3 ligase activity. (2) Higher oligomerization of TRIM32 proteins is readily form spherical hollow inclusions known as cytoplasmic bodies (CBs). (3) Ubiquitin is a common component of CB droplets and ubiquitination cascade promotes the formation of CBs. Therefore, we deduced that the TRIM32 protein oligomerization and CBs formation might be crucial for its biological functions. In other words, the failure to form CBs might imply the impaired oligomerization ability, reduced catalytic activity and abnormal physiological function.

In subcellular localization assay, we transfected the TRIM32-WT and mutants expression plasmids into HEK-293T cells and observed the formation of CBs by confocal microscopy. Both TRIM32-WT and the P130S mutant exhibited numerous fluorescent speckles in the cytoplasm, indicating normal higher-order oligomerization. In contrast, higher-order oligomerization status was disrupted to varying extents in the other 4 mutants. For the R394H and D487N mutants, the majority of fluorescent signals were diffused throughout the cytoplasm with very few small fluorescent speckles. In V591M and P619S mutants, only evenly dispersed cytoplasmic fluorescent signals were observed (Fig. 3A). Additionally, we performed co-transfected experiment to evaluate protein oligomerization status when WT protein and mutant protein co-present. Overlapping fluorescence signals of pmCherry-WT CBs and GFP-mutant CBs indicated that TRIM32-WT protein could interact with mutant TRIM32 protein, thereby enhancing oligomer formation. However, in WT + P130S and WT + R394H co-transfected cells, large sized CBs were observed, while only small or tiny dots were present in WT + D487N, WT + V591M and WT + P619 cells (Fig. 3B). This result might imply that the latter 3 variants have a more severe impact on protein oligomerization.

Impaired oligomerization ability of mutant TRIM32 proteins was quantitatively determined

The formation of CBs is an effective indicator reflects to oligomeric state [23], but it is difficult to quantify. Given that protein self-interaction is a necessary prerequisite for protein oligomerization, the ability of proteins to self-interact can be considered a substitute for their oligomerization capability. To roughly measure the self-interaction ability of mutant TRIM32 proteins, we employed a co-immunoprecipitation assay. Plasmids with FLAG tag and homologous plasmids with GFP tag were co-transfected into HEK-293T cells and an antibody against FLAG was used to generate the immunoprecipitate. The weaker band signals observed in the R394H, D487N, V591M, and P619S mutants indicated reduced self-interaction, indirectly suggesting that the oligomerization ability of these mutant proteins was partially impaired. However, quantification showed that the impact on self-interaction among the four variants was similar, with no significant differences. (Fig. 4A).

In order to more accurately determine the effect of the 4 missense variants on self-interaction ability, quantitative fluorescence resonance energy transfer (FRET) measurements were performed in living cells co-expressing ECFP-tagged and EYFP-tagged TRIM32 proteins. Figure 4B showed the fluorescence images of representative

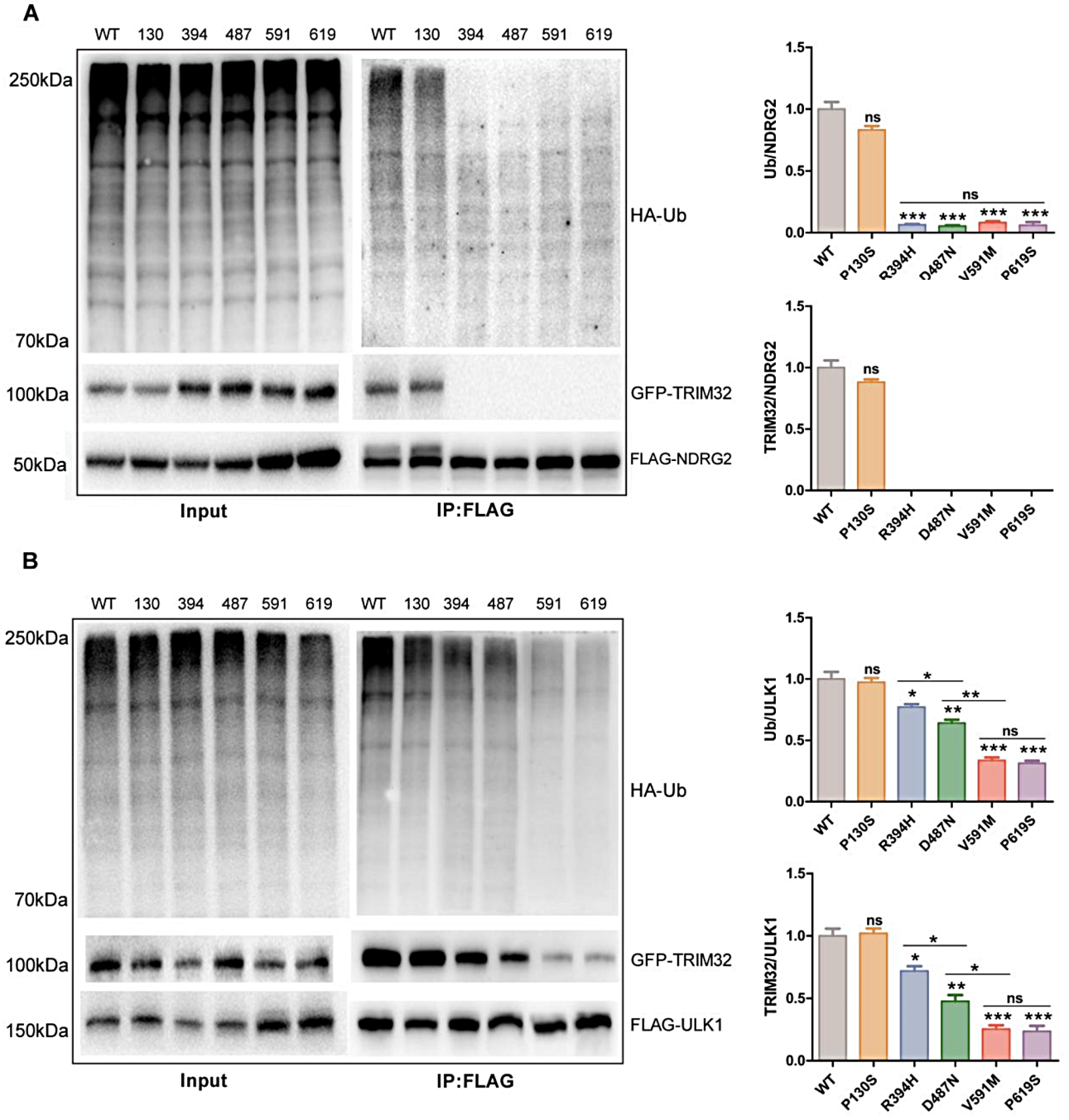

Fig. 2 Interaction and ubiquitination detection between TRIM32 and its substrate. (**A**) Left panel: Flag-NDRG2 was immunoprecipitated from HEK293T cells expressing HA-ubiquitin and either TRIM32-WT, P130S, D487N, R394H, V591M or P619S. Immunoprecipitated NDRG2 was probed for the presence of conjugated TRIM32 and HA-ubiquitin by western blot. Right panel: Protein grey value analysis performed using ImageJ, and the data are presented as means±SEMs. (**B**) Left panel: Flag-ULK1 was immunoprecipitated from HEK293T cells expressing HA-ubiquitin and either TRIM32-WT, P130S, D487N, R394H, V591M or P619S. Immunoprecipitated ULK1 was probed for the presence of conjugated TRIM32 and HA-ubiquitin by western blot. Right panel: Protein grey value analysis performed using ImageJ, and the data are presented as means±SEMs. A high molecular weight smear is seen on the HA blot indicative of high ubiquitination. Student's T-tests were performed to analyze the data and all data are shown as three biological replicates. "*" on the histogram columns represents the significant differences between each variant and WT; "*" on the horizontal line represents the significant differences of the variants below it. *$P < 0.05$; **$P < 0.01$; ***$P < 0.001$; ns, no significance

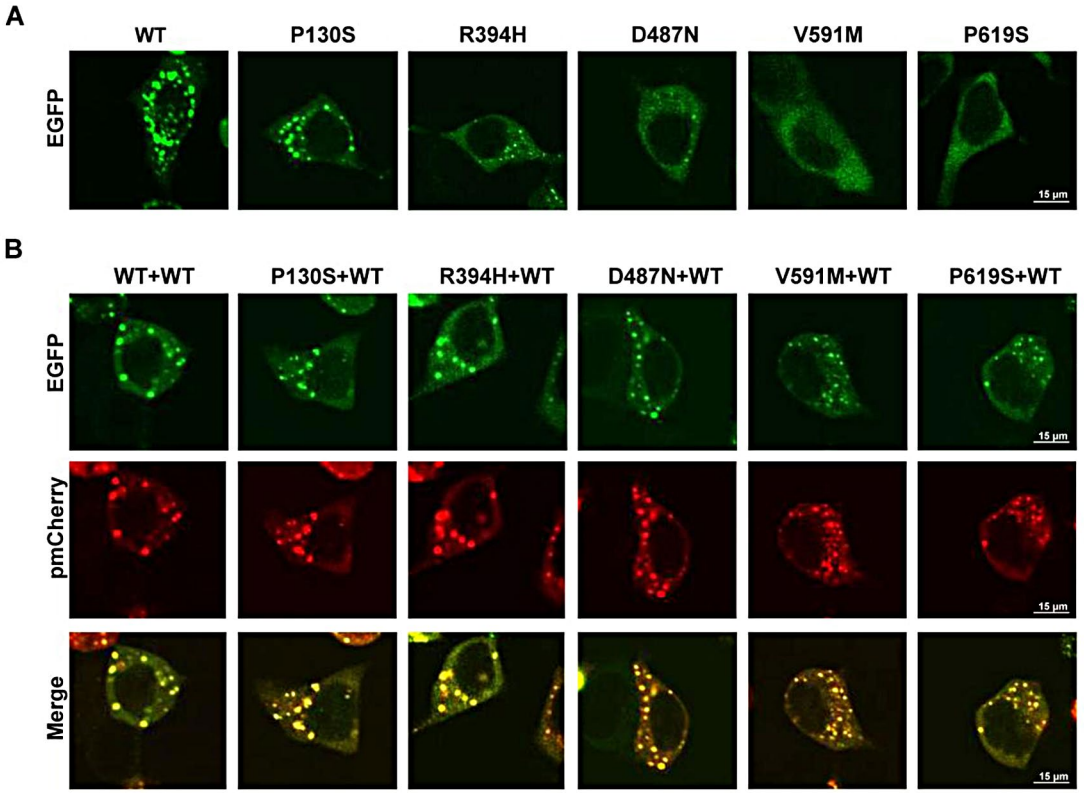

Fig. 3 Subcellular distribution of TRIM32 protein. (**A**) Localization of TRIM32-WT-EGFP and mutants in HEK-293T cell. HEK-293T cells were transfected with TRIM32-WT-EGFP, P130S-EGFP, 487 N-EGFP, R394H-EGFP, V591M-EGFP and P619S-EGFP. (**B**) Co-localization of TRIM32-EGFP mutants and TRIM32-WTpmCherry in HEK-293T cells. TRIM32-EGFP mutants and TRIM32-WT-pmCherry were transfected into HEK-293T cells. TRIM32-EGFP mutants protein can be found in aggregates that co-localize with the TRIM32-WT -pmCherry fluorescence, which appear yellow in the merged image. Scale bar = 15 μm (40× magnification)

cells co-expressing CFP-TRIM32 and YFP-TRIM32 in the WT and mutant types, and the corresponding pixel-to-pixel pseudo-color E_D (Donor-centric FRET efficiency) and Rc (acceptor–donorratio) images as well as their histograms. The six E_D–RC binding curves from at least 100 cells were saturable when Rc was larger than 4, and the EDmax (the index used to measure interaction strength) was calculated using the formula described in previous research (Fig. 4C) [17]. As predicted (Fig. 4D), TRIM32-WT had the highest $E_D$max value (0.45), indicating the strongest self-interaction ability. The TRIM32-P130S mutant has similar self-interaction ability with an $E_D$max value of 0.42. The E_D-Vmax value of the other variants was significantly reduced and displayed certain differences in such order: R394H(0.37) > D487N(0.26) > P619S(0.19) ≈ V591M(0.17), indicating that R394H mutant protein had the least effect on the oligomerization ability, the D487N mutant protein also retained a certain oligomerization ability, and the V591M and P619S mutant proteins severely lost the oligomerization ability. Interestingly, this order of degree of impaired oligomerization ability corresponded to the order of disease severity in homozygous patients.

Discussion

Accurate diagnosis is the first crucial step in effective clinical management to all diseases. For common diseases, diagnosis is typically based on the phenotype of the patients, such as characteristic clinical symptoms and positive laboratory findings. However, for monogenic diseases, where the causative agents are pathogenic gene mutations, molecular diagnosis of disease-causing DNA variants has become the mainstream approach due to advances in molecular biology techniques. Implementing reliable molecular diagnosis relies on identification of the causative genes and clear elucidation of the genotype-phenotype correlations. In other words, understanding which genotype corresponds to which phenotype is essential for accurate diagnosis of monogenic diseases. This is especially important in the area of prenatal diagnosis, where many types of disease phenotypes do not manifest during the fetal stage. Clinicians often determine whether a fetus is affected based solely on its genotype. A clear genotype-phenotype correlation analysis facilitates precise diagnosis for patients with monogenic diseases, thereby guiding clinicians' informed decision-making regarding patient care and treatment.

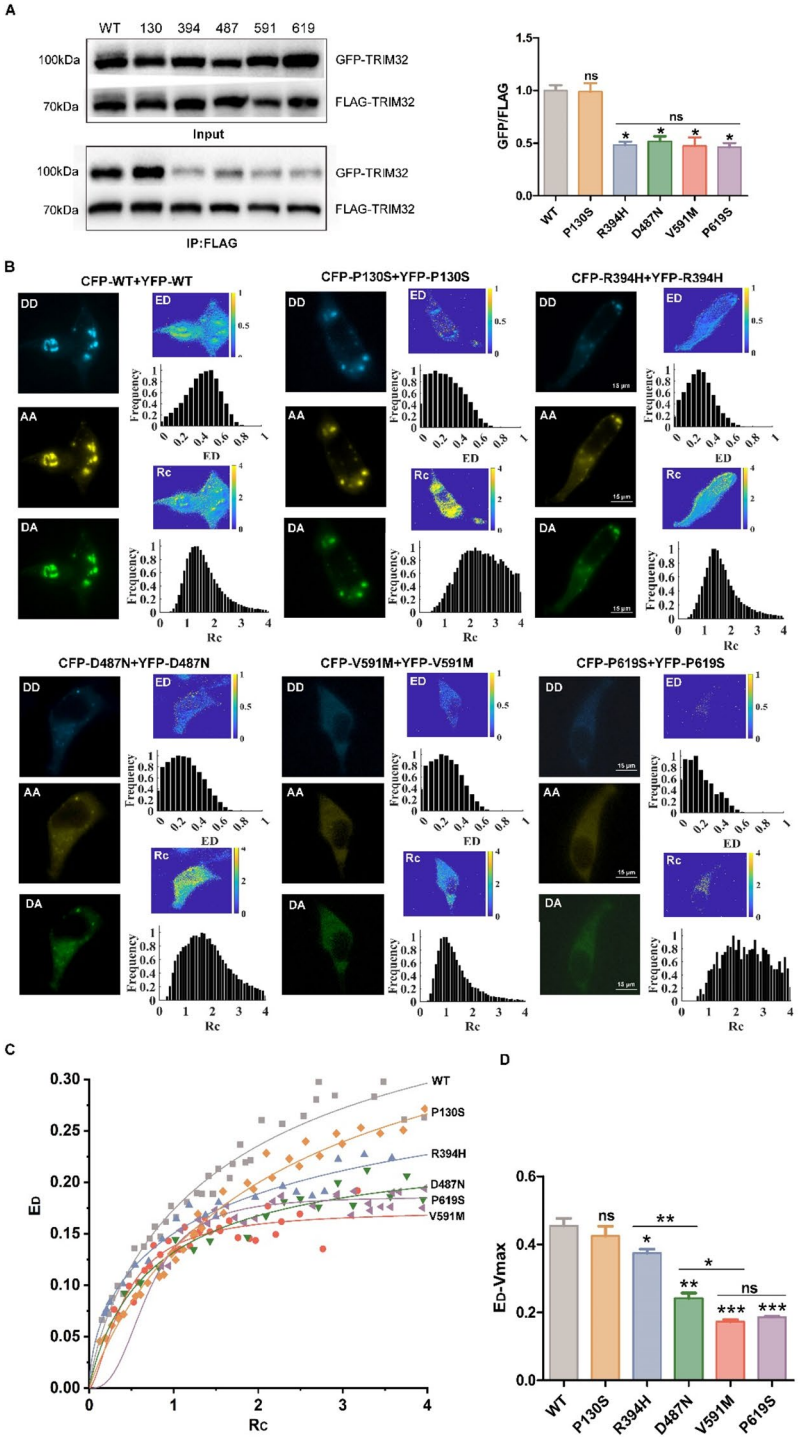

Fig. 4 Detection and FRET quantitative analysis of oligomerization of TRIM32. (**A**) Left panel: Co-IP-mediated analysis of TRIM32 self-interaction. HEK293T cells were transfected with Flag-tagged TRIM32, P130S, R394H, D487N, V591M or P619S and their EGFP-tagged counterparts. Immunoprecipitated Flag-tagged proteins were probed for the presence of conjugated EGFP-tagged proteins by western blot. Right panel: Protein grey value analysis performed using ImageJ, and the data are presented as means±SEMs. (**B**) The fluores-cence images of representative cells and the corresponding pseudo-color ED and Rc images as well as their histograms. Scale bar =15 μm (40× magnification). (**C**) The corrresponding ED-Rc plot from at least 100 cells. The saturation binding curves were fitted using Origin with the function: ED=EDmax × Rc/(Kd+Rc). (**D**) Statistical analysis of ED-Vmax. ED-Vmax is the maximum ED corresponding to saturation of donor binding sites by an acceptor. Student's T-tests were performed to analyse the data of each variant and WT. all data are shown with error bars (±SEMs). "*" on the histogram columns represents the significant differences between each variant and WT; "*" on the horizontal line represents the significant differences of the variants below it. *$P < 0.05$; **$P < 0.01$; ***$P < 0.001$; ns, no significance

For monogenic diseases with high incidence such as Duchenne muscular dystrophy, it is relatively straightforward to explain genotype–phenotype correlation by analyzing genotype and phenotype data from a large number of patients [24, 25]. However, for some rare diseases that showed high genetic heterogeneity and phenotypic diversity, the limited number of cases makes it challenging to establish correlation between mutation combination of disease-causing gene (genotype) and disease severity (phenotype). This limitation complicates targeted genetic counseling and necessitates alternative approaches to analyze genotype-phenotype correlations. In this study, we proposed a new analytical strategy in LGMD R8 to reveal genotype-phenotype correlations. By integrating results from bioinformatics analysis, cellular functional experiments, and biophysical assays, we aimed to provide new analytical strategy to better reveal these correlations.

Previous research [6–8, 26] on LGMD R8 and its causative gene TRIM32 had suggested: (1) LGMD R8 patients exhibit considerable heterogeneity in genetic background and clinical presentation. The plethora of mutation combinations (genotype) may explain the diversity of phenotypes, but it is not yet feasible to predict clinical severity based on genotypic data. (2) The biological function of TRIM32 as an E3 ubiquitin ligase, mediating the proteasomal degradation of target proteins, plays an important role in muscular physiology and pathology. (3) TRIM32 protein tends to oligomerize, and this oligomeric state is crucial for its E3 ligase catalytic activity. (4) LGMD R8 pathological variants cluster in the TRIM32 NHL domain, which mainly mediates TRIM32 oligomerization and interactions with substrates. In addition, based on current case data, we had following findings: (1) Patients carrying two variants in the NHL repeats usually present more severe symptoms than other patients [11]. (2) Homozygotes of missense variants in the NHL repeats were the largest group (Figure S1), and they displayed gradient divergence in two key disease severity indices, onset age and AWA (Fig. 1B). Hence, we hypothesized that a simple genotype-phenotype correlation could be established in these patients by analyzing the association between oligomeric status, catalytic activity, and disease severity. It had been reported that the severity of hemolysis in hereditary elliptocytosis (HE) patients was related to the percentage of dimeric spectrin (SpD) in the red blood cell membranes [27]. We propose that the clinical phenotype of LGMD R8 might similarly correlate with the degree of TRIM32 protein oligomerization in cells. In that case, a quantitative assessment of oligomerization capacity could potentially be used to predict disease severity.

Firstly, by compiling data on genotypes and corresponding impaired mobility phenotype in the patients(Fig. 1B), we found that: homozygotes of R394H variant had a mild phenotype with the latest onset age and could still walk at the age of 60; homozygotes of D487N variant showed moderate phenotype with intermediate onset age and wheelchair dependence in middle age; homozygotes of V591M variant and P619S variant displayed severe phenotypes with the earliest onset age and wheelchair dependence before the age of 30. In silico prediction analysis (Fig. 1D) also confirmed that the order of the degree of impact on protein structure and stability, from lowest to highest, was R394H, D487N, V591M and P619S. Ubiquitinating function experiments showed that mutant proteins had different effects on different substrates (Fig. 2). Binding of these 4 mutants with NDRG2 was severely affected, whereas interaction and ubiquitin activity to ULK1 were partially impaired. Notably, consistent with our hypothesis, the extent of changes in biochemical function caused by the 4 variants corresponded to the phenotypic severity. Meanwhile, we identified the oligomeric status of TRIM32 protein by observing the formation of CBs in cells (Fig. 3). Subcellular localization assay showed that formation of CBs was disrupted to varying extents in 4 mutants, indirectly proving that a decrease in E3 ligase activity was indeed accompanied by a decrease in higher-order oligomerization. Finally, we performed Co-IP and FRET experiment to confirm the impaired oligomerization ability caused by 4 mutants (Fig. 4). It should be emphasized that EDmax Value from FRET assay could be used to quantify the oligomerization capacity, and according to this result, the order of degree of impaired oligomerization ability corresponded to the order of disease severity as well. Taken together, we proposed a possible pathogenic mechanism of homozygous missense variants in NHL domain (Fig. 5), and proved our hypothesis that a distinct association existed between clinical severity, protein biological function, and protein oligomerization in these patients.

Conclusion

This study is the first to aim at elucidating a clear genotype-phenotype correlation of LGMD R8 disease. Our research achieved two objectives. In the field of medical genetics, we addressed the gap regarding the unknown association between TRIM32 genotype and LGMD R8 phenotype. Our innovative analytical strategy overcame the limitations posed by a limited number of cases, providing new insights for the study of related diseases. In the realm of clinical management for LGMD R8 patients, we offer a more accurate method to predict disease severity when encountering individuals with known or unreported variants in the NHL domain. Learning their disease progression prior to the onset of symptoms will promote patients' awareness of avoiding excessive exercise and maintaining existing muscle function, improving their quality of life. Moreover, in genetic

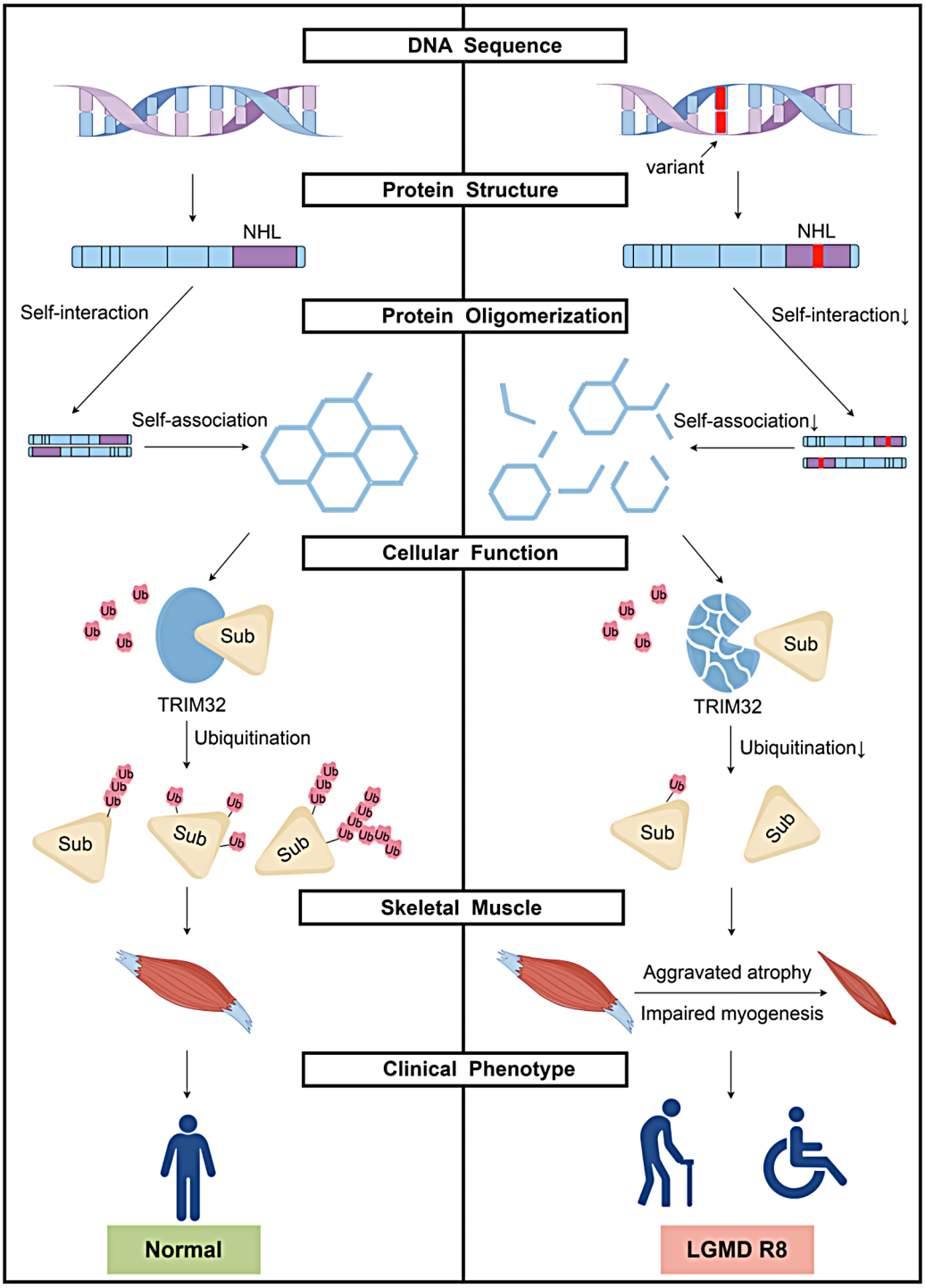

Fig. 5 Pathogenic mechanism of missense variants in NHL domain of TRIM32 gene. Variants in the NHL domain of TRIM32 lead to impaired oligomerization and structural stability of the protein, subsequently hindering interaction and ubiquitination with critical substrates essential for maintaining muscle homeostasis. This cascade ultimately results in muscle atrophy and impaired muscle regeneration, with a clinical phenotype of proximal muscle weakness, and in severe cases, reliance on walking aids or wheelchairs for travel. NHL domain (purple on TRIM32): mediates oligomerization; TRIM32 (blue): interaction and ubiquitination with substrates; Substrate (yellow): related to muscle homeostasis. The material of the figure is provided by figdraw2.0

counseling for families with affected fetuses, clinicians could offer additional information on the future phenotype of the fetus, which is a valuable reference for parental decision-making.

Abbreviations

LGMD R8	limb-girdle muscular dystrophy R8
AWA	age of any walking aid
LGMDs	limb-girdle muscular dystrophies
CK	creatine kinase
Ub	ubiquitin
BBS	Bardet-Biedl syndrome
WT	wild-type
cDNA	complementary DNA
HEK	human embryonic kidney
FBS	fetal bovine serum
Co-IP	co-immunoprecipitation
CBs	cytoplasmic bodies
FRET	fluorescence resonance energy transfer
HE	hereditary elliptocytosis
SpD	dimeric spectrin

Supplementary Information

The online version contains supplementary material available at https://doi.org/10.1186/s40478-025-01971-8.

Supplementary Material 1

Supplementary Material 2

Acknowledgements
Not applicable.

Author contributions
Xiongda Liang: Conceptualization, Investigation, Formal analysis, Writing - Original draft, Writing - Review&Editing. Jiameng Si: Conceptualization, Methodology, Formal analysis. Hongting Xie: Methodology, Formal analysis. Yuqing Guan: Methodology, Writing - Review & Editing. Wanying Lin: Methodology, Writing - Review & Editing. Zezhang Lin: Methodology, Formal analysis. Ganwei Zheng: Methodology. Xiaofeng Wei: Resources, Project administration. Xingbang Xiong: Methodology, Software. Zhengfei Zhuang: Methodology, Software.Xuan Shang: Conceptualization, Resources, Writing - Review&Editing, Funding acquisition.

Funding
This research was supported by research funding from National Natural Science Foundation of China (82370122), Guangdong Basic and Applied Basic Research Foundation (2024A1515012748).

Data availability
No datasets were generated or analysed during the current study.

Declarations

Ethics approval and consent to participate
Not applicable.

Consent for publication
Not applicable.

Competing interests
The authors declare no competing interests.

Received: 10 October 2024 / Accepted: 21 February 2025
Published online: 04 March 2025

References

1. Georganopoulou DG, Moisiadis VG, Malik FA, Mohajer A, Dashevsky TM, Wuu ST, Hu CK (2021) A journey with LGMD: from protein abnormalities to patient impact. Protein J 40(4):466–488
2. Angelini C (2020) LGMD. Identification, description and classification. Acta Myol 39(4):207–217
3. Jerusalem F, Engel AG, Gomez MR (1973) Sarcotubular myopathy. A newly recognized, benign, congenital, Familial muscle disease. Neurology 23(9):897–906
4. Shieh PB, Kudryashova E, Spencer MJ (2011) Limb-girdle muscular dystrophy 2H and the role of TRIM32. Handb Clin Neurol 101:125–133
5. Johnson K, De Ridder W, Topf A, Bertoli M, Phillips L, De Jonghe P, Baets J, Deconinck T, Rakocevic Stojanovic V, Peric S et al (2019) Extending the clinical and mutational spectrum of TRIM32-related myopathies in a non-Hutterite population. J Neurol Neurosurg Psychiatry 90(4):490–493
6. Kumarasinghe L, Xiong L, Garcia-Gimeno MA, Lazzari E, Sanz P, Meroni G (2021) TRIM32 and Malin in neurological and neuromuscular rare diseases. Cells 10(4)
7. Jeong SY, Choi JH, Kim J, Woo JS, Lee EH (2023) Tripartite Motif-Containing protein 32 (TRIM32): what does it do for skeletal muscle?? *Cells* 12(16)
8. Bawa S, Piccirillo R, Geisbrecht ER (2021) TRIM32: A multifunctional protein involved in muscle homeostasis, glucose metabolism, and tumorigenesis. Biomolecules 11(3)
9. Sardiello M, Cairo S, Fontanella B, Ballabio A, Meroni G (2008) Genomic analysis of the TRIM family reveals two groups of genes with distinct evolutionary properties. BMC Evol Biol 8:225
10. Chiang AP, Beck JS, Yen HJ, Tayeh MK, Scheetz TE, Swiderski RE, Nishimura DY, Braun TA, Kim KY, Huang J et al (2006) Homozygosity mapping with SNP arrays identifies TRIM32, an E3 ubiquitin ligase, as a Bardet-Biedl syndrome gene (BBS11). Proc Natl Acad Sci U S A 103(16):6287–6292
11. Guan Y, Liang X, Li W, Lin W, Liang G, Xie H, Hou Y, Hu Y, Shang X (2023) TRIM32 biallelic defects cause limb-girdle muscular dystrophy R8: identification of two novel mutations and investigation of genotype-phenotype correlation. Skelet Muscle 13(1):10
12. Lazzari E, Meroni G (2016) TRIM32 ubiquitin E3 ligase, one enzyme for several pathologies: from muscular dystrophy to tumours. Int J Biochem Cell Biol 79:469–477
13. Cevik S, Wangtiraumnuay N, Van Schelvergem K, Tsukikawa M, Capasso J, Biswas SB, Bodt B, Levin AV, Biswas-Fiss E (2023) Protein modeling and in Silico analysis to assess pathogenicity of ABCA4 variants in patients with inherited retinal disease. Mol Vis 29:217–233
14. Hoppe A, Christensen K, Swanson JA (2002) Fluorescence resonance energy transfer-based stoichiometry in living cells. Biophys J 83(6):3652–3664
15. Erickson MG, Alseikhan BA, Peterson BZ, Yue DT (2001) Preassociation of calmodulin with voltage-gated Ca(2+) channels revealed by FRET in single living cells. Neuron 31(6):973–985
16. Yang F, Qu W, Du M, Mai Z, Wang B, Ma Y, Wang X, Chen T (2020) Stoichiometry and regulation network of Bcl-2 family complexes quantified by live-cell FRET assay. Cell Mol Life Sci 77(12):2387–2406
17. Ben-Johny M, Yue DN, Yue DT (2016) Detecting stoichiometry of macromolecular complexes in live cells using FRET. Nat Commun 7:13709
18. Di Rienzo M, Antonioli M, Fusco C, Liu Y, Mari M, Orhon I, Refolo G, Germani F, Corazzari M, Romagnoli A et al (2019) Autophagy induction in atrophic muscle cells requires ULK1 activation by TRIM32 through unanchored K63-linked Polyubiquitin chains. Sci Adv 5(5):eaau8857
19. Mokhonova EI, Avliyakulov NK, Kramerova I, Kudryashova E, Haykinson MJ, Spencer MJ (2015) The E3 ubiquitin ligase TRIM32 regulates myoblast proliferation by controlling turnover of NDRG2. Hum Mol Genet 24(10):2873–2883
20. Tozawa T, Matsunaga K, Izumi T, Shigehisa N, Uekita T, Taoka M, Ichimura T (2022) Ubiquitination-coupled liquid phase separation regulates the accumulation of the TRIM family of ubiquitin ligases into cytoplasmic bodies. PLoS ONE 17(8):e0272700
21. Locke M, Tinsley CL, Benson MA, Blake DJ (2009) TRIM32 is an E3 ubiquitin ligase for dysbindin. Hum Mol Genet 18(13):2344–2358
22. Koliopoulos MG, Esposito D, Christodoulou E, Taylor IA, Rittinger K (2016) Functional role of TRIM E3 ligase oligomerization and regulation of catalytic activity. EMBO J 35(11):1204–1218
23. Ganser-Pornillos BK, Chandrasekaran V, Pornillos O, Sodroski JG, Sundquist WI, Yeager M (2011) Hexagonal assembly of a restricting TRIM5alpha protein. Proc Natl Acad Sci U S A 108(2):534–539
24. Preethish-Kumar V, Shah A, Polavarapu K, Kumar M, Safai A, Vengalil S, Nashi S, Deepha S, Govindaraj P, Afsar M et al (2022) Disrupted structural

connectome and neurocognitive functions in Duchenne muscular dystrophy: classifying and subtyping based on Dp140 dystrophin isoform. J Neurol 269(4):2113–2125
25. Yuan R, Yi J, Xie Z, Zheng Y, Han M, Hou Y, Wang Z, Yuan Y (2018) Genotype-phenotype correlation in Becker muscular dystrophy in Chinese patients. J Hum Genet 63(10):1041–1048
26. Frosk P, Weiler T, Nylen E, Sudha T, Greenberg CR, Morgan K, Fujiwara TM, Wrogemann K (2002) Limb-girdle muscular dystrophy type 2H associated with mutation in TRIM32, a putative E3-ubiquitin-ligase gene. Am J Hum Genet 70(3):663–672
27. Coetzer T, Palek J, Lawler J, Liu SC, Jarolim P, Lahav M, Prchal JT, Wang W, Alter BP, Schewitz G et al (1990) Structural and functional heterogeneity of alpha spectrin mutations involving the spectrin heterodimer self-association site: relationships to hematologic expression of homozygous hereditary elliptocytosis and hereditary pyropoikilocytosis. Blood 75(11):2235–2244

Publisher's note